Nuclear Engineering and Technology 55 (2023) 1988–1993

Contents lists available at ScienceDirect

Nuclear Engineering and Technology

journal homepage: www.elsevier.com/locate/net

Original Article

# Effect of silica fume content in concrete blocks on laser-induced explosive spalling behavior

Seong Y. Oh*, Gwon Lim, Sungmo Nam, Byung-Seon Choi, Taek Soo Kim, Hyunmin Park

*Korea Atomic Energy Research Institute, 111, Daedeok-daero 989beon-gil, Yuseong-gu, Daejeon, 34057, Republic of Korea*

ARTICLE INFO

*Article history:*
Received 17 November 2022
Received in revised form
2 February 2023
Accepted 2 March 2023
Available online 6 March 2023

*Keywords:*
Fiber laser decontamination
Laser scabbling
Laser-induced explosive spalling
High-strength concrete including silica fume
Thermal images

ABSTRACT

This experimental study investigated the effect of silica fume mixed in concrete blocks on laser-induced explosion behavior. We used a 5.3 kW fiber laser as a thermal source to induce explosive spalling on a concrete surface blended with and without silica fume. An analytical approach based on the difference in the removal rate and thermal behavior was used to determine the effect of silica fume on laser-induced explosive spalling. A scanner was employed to calculate the laser-scabbled volume of the concrete surface to derive the removal rate. The removal rate of the concrete mixed with silica fume was higher than that of without silica fume. Thermal images acquired during scabbling were used to qualitatively analyze the thermal response of laser-induced explosive spalling on the concrete surface. At the early stage of laser heating, an uneven spatial distribution of surface temperature appeared on the concrete blended with silica fume because of frequent explosive spalling within a small area. By contrast, the spalling frequency was relatively lower in laser-heated concrete without silica fume. Furthermore, we observed that a larger area was removed via a single explosive spalling event owing to its high porosity.


## 1. Introduction

Explosive spalling and surface rupture can occur in concrete which absorbs intense thermal energy [1,2]. It involves releasing debris into the atmosphere. In detail, concrete exposed to intense thermal heating evaporates the internal moisture rapidly, and the vapor generated is accumulated at the capillary pores. The excessive amount of vapor accumulated at the pores increases the pore pressure beyond the threshold value. This causes explosion in the pores, thus shattering the area around the pores into small pieces [3,4]. The porosity of concrete significantly affects the probability of inducing explosive spalling on its surface. For example, dense concrete, which is primarily distributed with micropores, provides an environment in which the vapor pressure increases rapidly in the pores of the concrete at high temperatures [4]. Thus, such a dense structure induces the accumulation of high pressures beyond the threshold, thereby increasing the possibility of explosive spalling. The porous structure in concrete is significantly affected by the water/binder (W/B) ratio and binder type [1]. In particular, silica fume in binder materials can fill the gaps between cement particles owing to its ultrafine grain size, which thereby reduces the porosity of concrete. The filling effect of silica fume contributes to the formation of dense concrete cured via the hydration process accompanying the pozzolanic reaction in ready-mixed concretes [5]. Therefore, concrete containing silica fume is more likely to undergo explosive spalling when exposed to high temperatures [6].

Laser light has been used as a thermal source to induce explosive spalling on concrete surfaces [7,8]. In fact, laser-induced explosive spalling can be used as a decontamination approach for removing radioactively contaminated concrete surfaces [9]. Laser scabbling is a decontamination technology that removes nuclear-contaminated concrete surfaces by inducing explosive spalling using a high-power laser beam [10]. Because this laser scabbling technique operates in a dry state, it can reduce the amount of concrete waste generated from decontamination process, which cannot be achieved with other technologies operating under wet conditions [11]. Furthermore, fiber-coupled laser scabbling tools are suitable for remote operations because of the compact size of the optical head, the extendable optical fiber, and the removal method, which does not require direct contact between the optical head and concrete surface [8]. Therefore, they can be used effectively at decontamination sites where remote operation is required to protect workers from radiation.

* Corresponding author.
*E-mail address:* syoh73@kaeri.re.kr (S.Y. Oh).

https://doi.org/10.1016/j.net.2023.03.002

We conducted a laser scabbling study to develop concrete decontamination technology. For concretes constructed under various mixing conditions, it is necessary to investigate various explosive responses induced by laser interaction to develop efficient laser decontamination technology. Few experimental studies have specifically investigated the effect of silica fume exerted on thermal spalling behavior of concrete using laser heating source [6]. In this study, we performed laser scabbling experiments on high-strength concrete blocks with and without silica fume content. A 5.3 kW fiber laser was used to trigger explosive spalling on both concretes. The spalling behaviors of the laser-heated concretes were compared in terms of the removal rate and temperature response.

## 2. Materials and methods

### 2.1. Laser scabbling system

A high-power fiber laser (IPG YLS-5000, $\lambda = 1070$ nm) operated in continuous mode was used as a thermal source to induce explosive spalling on the concrete surface. A process fiber (core diameter: 600 μm; length: 20 m) was connected between the laser system and the optical head to feed a high power laser beam into a collimator ($f = 160$ mm) and a focusing lens ($f = 100$ mm) mounted at the head. The focused beam quality of the $M^2$ value was measured to be 62.2 using a FocusMonitor (PRIMES GmbH) at an actual maximum laser power of 5.3 kW. The divergence angle and waist radius of the focused laser beam were 12.9° and 187 μm, respectively. The stand-off distance between the nozzle tip and concrete block surface was fixed at 400 mm. As shown in Fig. 1, the optical head coupled to the X–Y–Z stage was set to propagate along a programmed path on the concrete block surface. Thermal images were obtained using a thermal imaging camera (FLIR A 615) at a distance of 1.3 m from the concrete block.

### 2.2. Specimen preparation

Table 1 presents the composition of the ready-mixed concretes used in this study. Two types of concrete blocks were prepared using the same total binder content but different amount of silica fume. The W/B and fine aggregate ratio (S/a) were 0.34 and 0.472, respectively, which were the same for both concretes. Crushed limestone and siliceous sand were used as coarse and fine aggregates, respectively. The binding material comprised ASTM (American Society for Testing and Materials) Type I ordinary Portland cement, ASTM grade 80 blast furnace slag, ASTM class F fly ash, and densified silica fume. The silica fume content of specimen SF20 accounted for 20% by weight of the binder [6]. Specimen SF0 was composed of concrete without silica fume. A polycarboxylate-type superplasticizer (SP450, Fosrock Korea Inc., Republic of Korea) was used to improve the workability of the prepared mixtures. After pouring the fluid ready-mix into cuboid molds (height and width: 300 mm; thickness: 80 mm), they were stored in mold for 1 d [12]. After demolding, the specimens were stored in a tank filled with saturated lime solution (20 ± 2 °C) for 27 d.

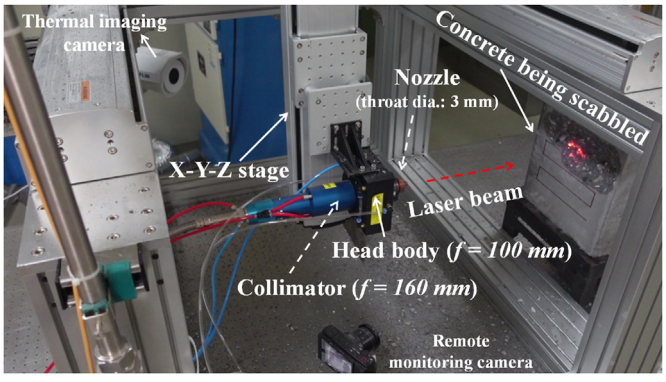


**Fig. 1.** Setup for the laser scabbling experiment.

Based on the ASTM C 39 Standard Test Method for Compressive Strength of Cylindrical Concrete Specimens, the 28-d compressive strength was measured using a hydraulic compressive strength test machine (S1 Industry Co., Korea, S1-1471D) [12]. Each three specimens of SF0 and SF20 were tested to obtain their compressive strength. The loading was controlled by displacement (2.5 mm/min). The compressive strength of SF0 and SF20 specimens was measured to be 58 ± 1.46 Mpa and 43 ± 1.25 Mpa, respectively [13–15].

### 2.3. Measurement of removal rates of scabbled specimens

The removed volume in the scabbling process was obtained via two methods. First, the removed volume was measured using two three-dimensional (3D) scanner devices [8]: Artec eva (Artec3D) and laser-probed Global Advantage 9.12.8(HEXAGON). Subsequently, SolidWorks and PolyWorks programs were used to calculate the removed concrete volume by converting the 3D scanned data into a solid model. In the second approach, the removed volume was calculated based on the difference in the weight of the concrete blocks before and after scabbling [12,16]. The removal rates were calculated from the removed volume and the overall laser firing time.

## 3. Results and discussion

Laser scabbling experiments on concrete blocks were performed to examine the effect of silica fume on the explosive spalling behavior. Fig. 2(a) and (c) present the laser-spalled concrete blocks of SF0 and SF20, respectively. A 5.3 kW laser beam was launched at a speed of 200 mm/min on the concrete surface along a 200 mm (length) × 40 mm (width) programmed path. The weak pink light shown in Fig. 2(a) and (c) indicates the existence of laser light, which was captured by a remote camera sensitive to infrared light. The laser beam, with a radius of 45 mm at a stand-off distance of 400 mm, oscillated sideways with approximately one-half overlap on the concrete surface. The total scabbled area exceeded 200 mm in length and 160 mm in width. The beam diameter and laser intensity impacting the concrete surface were calculated to be 90 mm and 83 W/cm$^2$, respectively. Energetic explosive spalling was observed in both concrete blocks even with the injection of a low-intensity laser beam. This was because the low W/B ratio created low porosity in the concrete [1]. Consequently, it reduced the permeability in the internal structure, which improved the capability of trapping the laser-produced vapors at the pores [4]. It also provided an environment susceptible to explosive spalling in the pores even when they were filled with relatively small amounts of laser-produced vapor.

However, some differences were observed between the two specimens, as shown in Fig. 2(a) and (c). The size spalled by one sweep of the laser beam was slightly wider in specimen SF20 compared with specimen SF0. This indicated that specimen SF20 was more susceptible to explosive spalling even when it was in contact with the edge of a laser beam that had a relatively low intensity. Essentially, specimen SF20 exhibited a more sensitive spalling response to laser heating. The removal rates were measured to quantitatively compare the differences in the spalling response between the two laser-spalled specimens. The removal

**Table 1**
Composition of the ready-mixed concretes prepared for this study.

| | W/B | S/a (s/a,%) | Concrete materials (kg/m$^3$) | | | | | | | |
|---|---|---|---|---|---|---|---|---|---|---|
| | | | Water | Cement | Blast furnace slag | Fly ash | Silica Fume | Fine aggregate | Crushed coarse aggregate | Superplasticizer |
| SF0 | 0.34 | 47.2 | 160.2 | 280.0 | 140.0 | 47.0 | 0.0 | 822.0 | 920.0 | 5.1 |
| SF20 | 0.34 | 47.2 | 160.2 | 186.0 | 140.0 | 47.0 | 94.0 | 822.0 | 920.0 | 5.1 |

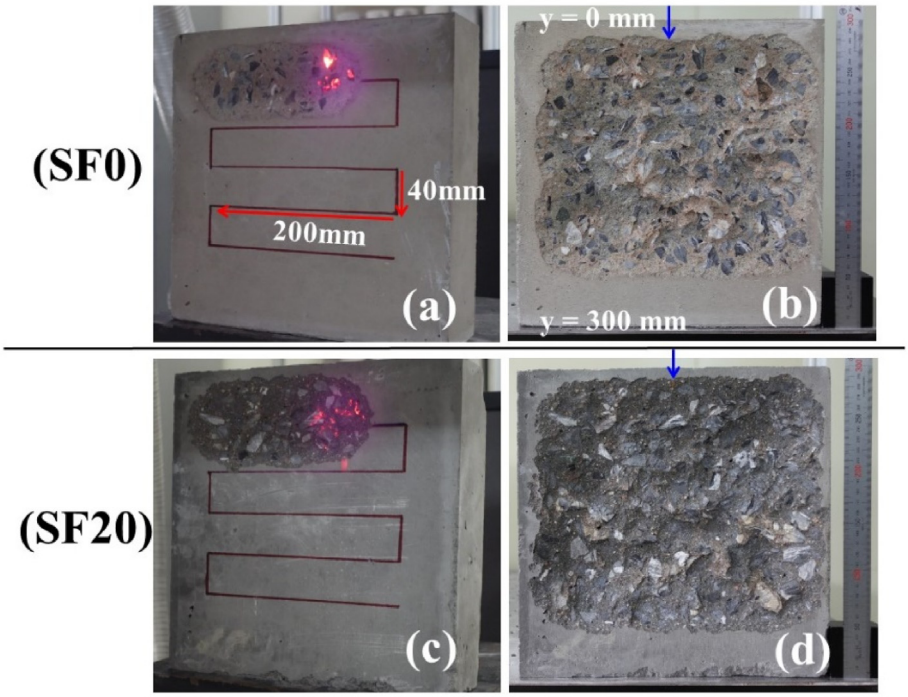


**Fig. 2.** (a), (c) Laser-spalled specimens SF0 and SF20. (b), (d) Specimens SF0 and SF20 after laser scabbling.

**Table 2**
Removal rates calculated using 3D scanners and the weight difference.

| Method | Removal rate (cm$^3$/min) | |
|---|---|---|
| | SF0 | SF20 |
| Artec eva | 89.0 | 117.7 |
| Global Advantage | 90.9 | 117.5 |
| Weight difference | 94.7 | 123.7 |

rates are listed in Table 2.

The removal rates of specimen SF20 were significantly higher than those of specimen SF0, which indicated that the laser-induced explosive spalling generated more debris in the concrete blended with silica fume. This was because silica fume with minute features further reduces the porosity of the cured concrete block. Meanwhile, other binder materials, such as blast furnace slag, fly ash, and cement particles, generally have particles sizes that are one to two orders of magnitude larger than those of silica fume particles [1]. Silica fume serves as a filler between other coarser binder particles during the hydration of ready mixed concrete, thus resulting in a denser concrete structure with finer pores. Therefore, vigorous explosive spalling is more likely to be induced in concrete containing silica fume. As can be seen in Table 2, the two 3D scanners yielded similar results. However, slightly higher removal rates were measured when the method based on the weight difference before and after scabbling was used. This might be caused by the weight loss uncertainty due to moisture evaporation from laser heating.

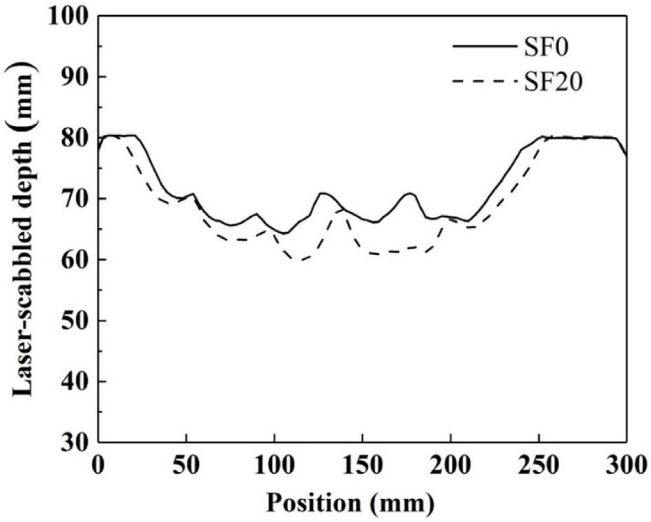


**Fig. 3.** Depth profiles of specimens SF0 and SF20 measured using a 3D scanner (Artec 3D).

The depth profile was investigated to compare the differences in the stripped shapes of the two concretes along the direction indicated by the blue arrow in Fig. 2(b) and (d). The depth profiles were calculated using mesh data measured using the 3D scanner (Artec

3D). Both profiles presented in Fig. 3 show parabolic shapes with uneven bottoms [8]. The edge regions, where the laser beam was irradiated only once, were spalled shallowly. Additionally, the surface removal degree of specimen SF20 containing silica fume was wider and deeper compared with that of the concrete without silica fume. The maximum peeling depth of specimen SF0 was 15 mm, whereas that of SF20 was 20 mm. This confirmed that explosive spalling was induced more actively in the concrete mixed with silica fume under the same laser-energy exposure conditions. The addition of silica fume contributed to further lowering the porosity, thereby further enhancing the impermeability in concrete. When exposed to the high temperatures, the reduced permeability promotes a quick accumulation of the vapor pressures at pores capable of inducing explosive spalling [17].

Fig. 4 shows the spatial distributions of the surface temperatures over time after the laser was fired and their corresponding histograms. The y-axis values in the histogram represent the number of pixels in the laser-heated area. Based on the thermal images presented in Fig. 4, evidently, the radius of the laser-spalled region of specimen SF20 was larger than that of specimen SF0. Considering that the energy intensity of the laser beam is relatively weaker at its edge, the finding above indicates that concrete mixed with silica fume was more susceptible to explosive spalling even when a lower thermal energy was involved. This is because specimen SF20 contained numerous fine pores, which caused a rapid increase in the vapor pressure even when a minute amount of water vapor was trapped in the pores.

Based on the histogram shown in Fig. 4(c), the surface temperature was evenly distributed in the range of 200–500 °C. However, some differences were observed between the two temperature distributions. As shown in Fig. 4(a) and (b), specimen SF0 exhibited less active spalling without explosion in the initial stage after the laser beam was launched. By contrast, an active spalling was observed in specimen SF20. This indicates that specimen SF20 responded more rapidly to laser heating. Furthermore, the vigorous explosions that occurred in specimen SF20 reduced the temperature. The SF20 specimen shown in Fig. 4(c) indicated a maximum value of pixel count at a lower temperature compared with the SF0 specimen.

After 2 s, frequent explosive spalling with a small removal area was more prevalent in specimen SF20. By contrast, less frequent explosions with relatively large spalling areas occurred in specimen SF0. Based on the histogram shown in Fig. 4(f), specimen SF20 exhibited a peak value of pixel count at approximately 300 °C. This was due to the numerous unheated micro-regions that were newly exposed to the atmosphere after extensive surface erosion due to frequent explosions. However, specimen SF0 exhibited a wider distribution without a distinct peak value owing to its less active spalling. After 4 s, active explosive spalling occurred in specimen SF0, as shown in Fig. 4(g). Based on the histogram shown in Fig. 4(i), specimen SF0 exhibited a peak temperature of approximately 350 °C, similar to specimen SF20. The number of counts for specimen SF20 was higher owing to its larger spalling area.

After laser scabbling, the scattered debris was gathered to examine the grain size distribution [6]. Fig. 5(a) and (c) show the debris accumulated after scabbling SF0 and SF20. A series of prepared sieves was stacked in the order of their mesh sizes. The mesh sizes were 4.7, 4, 2.8, 2, and 1 mm. The debris was placed into stacked sieves and agitated vertically to calculate the amount remaining in each sieve. Fig. 5(b) and (d) show the debris remaining in the sieve with a mesh size of 4.7 mm. The weight of the debris remaining in each sieve was measured. Table 3 lists the weight percentages of debris in order of the grain size. Debris over 4.7 mm constituted more than 33% of the total debris generated by both specimens. A considerable amount of this larger debris showed coarse aggregates bonded to the mortar. Explosive spalling occurred primarily in the pores of areas without coarse aggregates. The effect of explosive spalling at the pores might have contributed

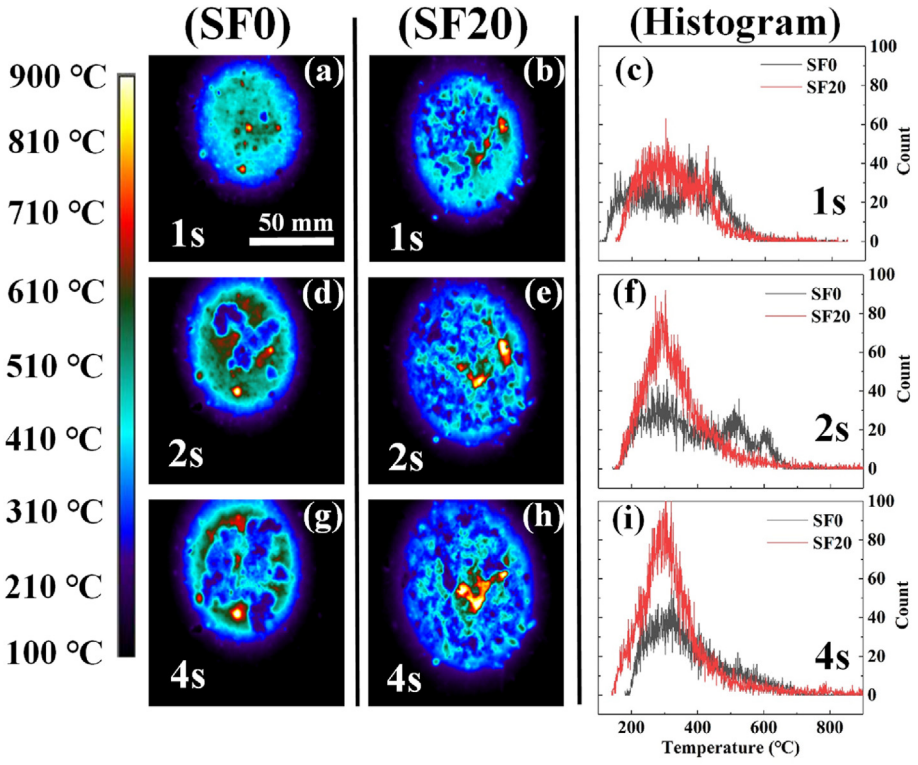


**Fig. 4.** Series of thermal images and histograms based on elapsed time after a laser was launched on specimens SF0 and SF20.

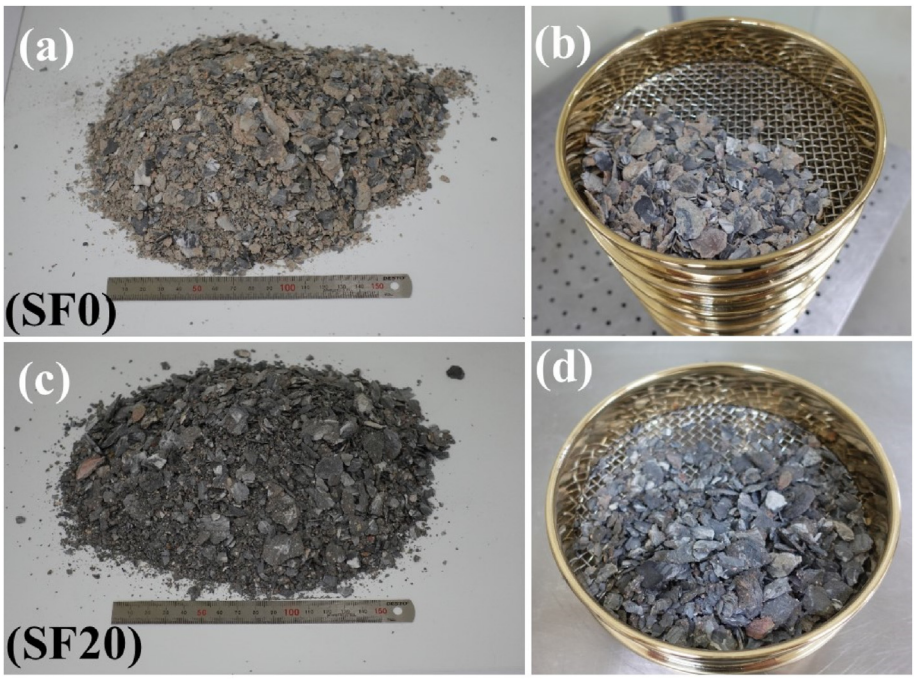


**Fig. 5.** (a), (c) Debris accumulated after laser scabbling of SF0 and SF20. (b), (d) Debris remaining in sieve with mesh size of 4.7 mm.

**Table 3**
Weight percentage of debris remaining in each sieve.

| Size range of debris | Specimen SF0 | Specimen SF20 |
|---|---|---|
| >4.7 mm | 33 % | 36 % |
| >4.0 mm and <4.7 mm | 3 % | 3 % |
| >2.8 mm and <4.0 mm | 12 % | 11 % |
| >2.0 mm and <2.8 mm | 12 % | 12 % |
| >1.0 mm and <2.0 mm | 19 % | 16 % |
| <1.0 mm | 20 % | 20 % |

to the partial removal of the adjacent coarse aggregates. Debris measuring less than 1.0 mm constituted 20% of the total debris generated by both specimens.

## 4. Conclusion

The presence of silica fume significantly affected the behavior of laser-induced explosive spalling on concrete surfaces. This finding was supported experimentally by the removal rate of the concrete surface containing silica fume, which was significantly higher in laser-scabbled SF20 specimens. Furthermore, the surface removal degree of specimen SF20 was deeper and wider. This might have been because the fine-sized silica fume contributed significantly to the formation of dense concrete with smaller pores. This implies that a fine pore structure can induce explosive spalling easily, even when the amount of trapped water vapor is low. The results of thermal image analysis confirmed that frequent explosive spalling with a small removal area was dominant in specimen SF20. The mixing of silica fume in concrete induced the formation of a fine pore structure and consequently provided an environment susceptible to active explosive spalling under exposure to thermal energy.

## Declaration of competing interest

The authors declare that they have no known competing financial interests or personal relationships that could have appeared to influence the work reported in this paper.

## Acknowledgements

This study was supported by the Korea Institute of Energy Technology Evaluation and Planning (KETEP) grant funded by the Korean government (Project name: Development of Contamination Telemeter and Laser Scabbling Devices for Surface Decontamination of Highly radioactive Concrete, Project no.: 20201510300110), Republic of Korea.

## References

[1] P.K. Metha, P.J.M. Monteiro, Concrete: Microstructure, Properties, and Materials, third ed., McGraw-Hill, New York, 1994, pp. 32–41.
[2] R. Jansson, Fire Spalling of Concrete: Theoretical and Experimental Studies, KTH Royal Institute of Technology, Stockholm, Sweden, 2013.
[3] L.T. Phan, Pore pressure and explosive spalling in concrete, Mater. Struct. 41 (2008) 1623–1632, https://doi.org/10.1617/s11527-008-9353-2.
[4] Y. Fu, L. Li, Study on mechanism of thermal spalling in concrete exposed to elevated temperatures, Mater. Struct. 44 (2011) 361–376, https://doi.org/10.1617/s11527-010-9632-6.
[5] J.M.R. Dotto, A.G. de Abreu, D.C.C. Dal Molin, I.L. Müller, Influence of silica fume addition on concretes physical properties and on corrosion behaviour of reinforcement bars, Cem. Concr. Compos. 26 (2004) 31–39.
[6] Y. Ju, Kaipei Tian, H. Liu, H.-W. Reinhardt, L. Wang, Experimental investigation of the effect of silica fume on the thermal spalling of reactive powder concrete, Construction Building Mater. 155 (2017) 571–583, https://doi.org/10.1016/j.conbuildmat.2017.08.086.
[7] P. Hilton, The Potential of High Power Lasers in Nuclear Decommissioning, WM 2010 Conference, Arizona, Phoenix, 2010, 10092.
[8] B. Peach, M. Petkovski, J. Blackburn, D.L. Engelberg, An experimental investigation of laser scabbling of concrete, Constr. Build. Mater. 89 (2015) 76–89, https://doi.org/10.1016/j.conbuildmat.2015.04.037.
[9] T. Hirabayashi, Y. Kameo, M. Myodo, Application of a laser to decontamination and decommissioning of nuclear facilities at JAERI, high power lasers in civil engineering and architecture, Proc. SPIE. 3887 (2000) 94–103.
[10] B. Peach, M. Petkovski, J. Blackburn, D.L. Engelberg, Laser scabbling of mortars, Constr. Build. Mater. 124 (2016) 37–44, https://doi.org/10.1016/j.conbuildmat.2016.07.038.
[11] P.O. Sullivan, J.G. Nokhamzon, E. Cantrel, Decontamination and dismantling of radioactive concrete structures, NEA News 28 (2010 27–29).
[12] S.U. Heo, J.H. Kim, S.Y. Oh, G. Lim, S.M. Nam, T.S. Kim, H.M. Park, Chul-Woo Chung, Effect of moisture content and mix proportion of concrete on efficiency of laser scabbling, Chung, Case Stud. Constr. Mater. 16 (2022), e01040 (P. c).
[13] A. Imam, V. Kumar, V. Srivastava, Review study towards effect of Silica Fume

on the fresh and hardened properties of concrete, Adv. Concr. Constr. 6 (2018) 145–157, https://doi.org/10.12989/ACC.2018.6.2.145.
[14] R. Duval, E.H. Kadri, Influence of silica fume on the workability and the compressive strength of high-performance concretes, Cement Concr. Res. 28 (1998) 533–547, https://doi.org/10.1016/S0008-8846(98)00010-6.
[15] A.M. Rashad, H. ED, H. Seleem, A.F. Shaheen, Effect of silica fume and slag on compressive strength and abrasion resistance of HVFA Concrete, Int. J. Concr. Struct. Mater. 8 (2014) 69–81, https://doi.org/10.1007/s40069-013-0051-2.
[16] S.Y. Oh, G. Lim, S. Nam, T. Kim, J. Kim, C. Chung, H. Park, S. Kim, Laser scabbling of a concrete block using a high-power fiber laser, J. Nucl. Fuel Cycle waste Technol. 19 (2021) 289–295, https://doi.org/10.7733/jnfcwt.2021.19.3.289.
[17] H.W. Song, S.W. Pack, S.H. Nam, J.-C. Jang, V. Saraswathy, Estimation of the permeability of silica fume cement concrete, Constr. Build. Mater. 24 (2010) 315–321, https://doi.org/10.1016/j.conbuildmat.2009.08.033.